The Journal of Physiology

Millisecond precision temporal encoding of stimulus features during cortically generated gamma oscillations in the rat somatosensory cortex

Thomas Bessaih[1,4], Michael J. Higley[2,3,4] and Diego Contreras[4]

[1] *Sorbonne Universités, UPMC Univ Paris 06, INSERM, CNRS, Neurosciences Paris Seine – Institut de Biologie Paris Seine (NPS – IBPS), 75005 Paris, France*
[2] *Department of Neuroscience, Kavli Institute for Neuroscience, Yale School of Medicine, New Haven, CT 06520, USA*
[3] *Program in Cellular Neuroscience, Neurodegeneration and Repair, Yale School of Medicine, New Haven, CT 06520, USA*
[4] *Department of Neuroscience, University of Pennsylvania Perelman School of Medicine, Philadelphia, PA 19104, USA*

Edited by: Kim Barrett & Jesper Sjöström

Key points

- Rodents explore their immediate environment using their whiskers. Such exploration leads to micromotions, which contain many high-frequency (50–200 Hz) components.
- High-frequency whisker motion is represented faithfully in the temporal structure of the spike trains of trigeminal neurons. However, the representation of high-frequency sensory inputs in cortex is not fully understood.
- By combining extracellular and intracellular recordings in the rat somatosensory cortex and thalamus, we show that high-frequency sensory inputs, either sinusoidal or white noise, elicit internally generated gamma (20–60 Hz) band oscillations in cortical networks.
- Gamma oscillations modulate cortical spike probability while preserving sub-millisecond phase relations with high-frequency sensory inputs.
- Consequently, our results indicate that millisecond precision stimulus-locked spiking activity and sensory-induced gamma oscillation can constitute independent multiplexed coding schemes at the single-cell level.

Abstract In the natural environment, tactile exploration often leads to high-frequency vibrations at the level of the sensory organs. Single-unit recordings of cortical neurons have pointed towards either a rate or a temporal code for representing high-frequency tactile signals. In cortical networks, sensory processing results from the interaction between feedforward inputs relayed from the thalamus and internally generated activity. However, how the emergent activity represents high-frequency sensory input is not fully understood. Using multisite single-unit, local field potential and intracellular recordings in the somatosensory cortex and thalamus of lightly sedated male rats, we measured neuronal responses evoked by sinusoidal and

Thomas Bessaih studied biology at Ecole Normale Supérieure (Paris). He then received his PhD in Neuroscience from University Pierre & Marie Curie where he focused on the cellular mechanisms underlying normal and pathological thalamic activities in Dr Nathalie Leresche's laboratory. He continued his scientific training as a postdoctoral fellow with Professor Diego Contreras at the University of Pennsylvania where he examined information processing in cortical networks. He has been senior lecturer at University Pierre & Marie Curie since September 2012.

DOI: 10.1113/JP275245

band-pass white noise whisker stimulation at frequencies that encompass those observed during texture exploration (50–200 Hz). We found that high-frequency sensory inputs relayed from the thalamus elicit both sub-millisecond stimulus-locked responses and internally generated gamma (20–60 Hz) band oscillations in cortical networks. Gamma oscillations modulate spike probability while preserving sub-millisecond phase relations with sensory inputs. Therefore, precise stimulus-locked spiking activity and sensory-induced gamma oscillations can constitute independent multiplexed coding schemes at the single-cell level.

(Received 14 September 2017; accepted after revision 13 December 2017; first published online 18 December 2017)
Corresponding author D. Contreras: Department of Neuroscience, University of Pennsylvania Perelman School of Medicine, 415 Curie Blvd, Philadelphia, PA 19106-6074, USA. Email: diegoc@pennmedicine.upenn.edu

Introduction

In the natural environment, sensory stimuli often have complex temporal structures that might include rapidly changing signals. For instance, when we scan finely textured surfaces such as silk or satin with our fingers, complex high-frequency (50–800 Hz) and texture-specific vibrations are elicited in the skin (Weber *et al.* 2013; Manfredi *et al.* 2014). These vibrations activate two types of sensory afferents, namely rapidly adapting superficial receptors and deep Pacinian receptors (Mountcastle *et al.* 1967; Talbot *et al.* 1968; Freeman & Johnson, 1982; Weber *et al.* 2013).

At the level of the somatosensory cortex of non-human primates, the amplitude of high-frequency vibrations is encoded by the firing rate of individual neurons (Hyvarinen *et al.* 1968; Mountcastle *et al.* 1969; Harvey *et al.* 2013). Alternatively, as illustrated by the well-known phase-locking of the neuronal discharge in area 3B to sinusoidal stimuli of up to 800 Hz, it is assumed that the frequency content of skin vibrations is encoded by the temporal patterning of the spiking activity with millisecond precision (Hyvarinen *et al.* 1968; Mountcastle *et al.* 1969; Harvey *et al.* 2013).

While human and non-human primates use their fingers to gather information about their nearby environment, rodents explore their immediate environment using their whiskers (Diamond *et al.* 2008). During texture discrimination tasks, such exploration leads to micromotions, which contain many high-frequency components (Ritt *et al.* 2008; Wolfe *et al.* 2008; Lottem & Azouz, 2009). High-frequency whisker micromotions faithfully activate trigeminal primary afferents and neurons in the trigeminal nucleus of the brainstem (PR5), which can precisely and reliably lock their discharge to the cycles of sinusoidal stimulations at frequencies of up to 1 kHz and 300 Hz, respectively (Deschênes *et al.* 2003; Jones *et al.* 2004). The axons of PR5 neurons form the lemniscal pathway that project into the ventral posterior medial nucleus of the thalamus (VPM). VPM neurons process information from multiple whiskers and innervate the primary sensory area of the somatosensory cortex (S1) and, more heavily, structures called barrels in layer IV (for a review, see Feldmeyer *et al.* 2013).

Although in anaesthetized animals, individual thalamic neurons do not discharge faithfully for sinusoidal whisker deflections above 20–40 Hz (Deschênes *et al.* 2003), one-to-one stimulus phase-locking was observed in cortical single units for stimulation frequencies up to 220 Hz (Ewert *et al.* 2008). Taken together, these results indicate that phase-locked discharges among an ensemble of VPM neurons allow the transmission of the high-frequency content of whisker micromotions observed during texture discrimination tasks.

In cortical networks, sensory processing results from the interaction between sensory inputs relayed from the thalamus and internally generated activity (Destexhe & Contreras, 2006; Hasenstaub *et al.* 2007; Buonomano & Maass, 2009; Alenda *et al.* 2010). However, how emergent activity such as gamma oscillations that have been observed in the barrel cortex of both anaesthetized and awake animals interact with high-frequency sensory inputs at the cellular level is not fully understood (Ewert *et al.* 2008, 2015; Vinck *et al.* 2015).

In the present study, using multisite single-unit, local field potential and intracellular recordings in the thalamus and the somatosensory cortex of rats, we investigated how neuronal population dynamics leading to internally generated oscillatory activity are modulated by high-frequency sinusoidal whisker deflections, and how these oscillations interact with stimulus-locked responses.

Methods

Ethical approval

The investigators understand the ethical principles under which *The Journal of Physiology* operates, and this work complies with *The Journal's* animal checklist. Experiments were conducted in accordance with the ethical guidelines of the National Institutes of Health and with the approval of the Institutional Animal Care and Use Committee of the University of Pennsylvania. Adult male Sprague–Dawley rats (280–350 g, $n = 42$) were purchased from Charles

River Laboratories and were group housed with *ad libitum* access to food and water in a 12 h light–12 h dark cycle and acclimatized for 2 weeks before the experiments.

Surgery and preparation

Animals were anaesthetized with isoflurane vaporized in pure oxygen (5% for induction, 2% during surgery) and artificially ventilated (80–100 breaths min^{-1}). Body temperature was maintained at 37°C via a servo-controlled heating blanket and rectal thermometer (Harvard Apparatus, Holliston, MA, USA). Dexamethasone (10 mg kg^{-1}, I.P.) and glycopyrrolate (20 mg kg^{-1} S.C.) were given pre-operatively, and bupivacaine (S.C.) was administered in the region to be incised 15 min prior to the first incision. Rats were placed in a stereotaxic apparatus, craniotomies were made directly above the barrel cortex (−1.0 to −3.0 mm A/P, 4.0–7.0 mm M/L) and the VPM (−3.0 mm A/P, 3.0 mm M/L), and the dura was resected.

After electrode placement, craniotomies were filled with a solution of 4% agar. Then isoflurane was replaced by fentanyl (10–40 μg kg^{-1}, I.P.) alone or mixed with medetomidine (10–20 μg kg^{-1}, I.P.) in order to maintain the animal in a sedated state. If the animals presented any sign of discomfort, isoflurane (0.25–1%) was added to supplement this anaesthesia regime. Once a stable sedation regime was achieved animals were subjected to neuromuscular blockade with gallamine triethiodide (20 mg kg^{-1}, I.M.) in order to avoid reflex twitching of the whiskers during stimulus presentation. At the end of the experiments, animals were killed with an overdose of Nembutal (200 mg kg^{-1}, I.P.).

Electrophysiological recordings

Cortical recordings of units and local field potentials (LFPs) were obtained using sharp-tipped multi-tetrode printed silicon probes (Neuronexus, Ann Arbor, MI, USA). The probe consisted of two shanks, separated horizontally by 150 μm, with two tetrodes each, separated vertically by 150 μm. Each tetrode was made of four recording sites. Recording sites had a diameter of 11 μm (∼1–2 MΩ impedance) and were spaced 25 μm apart. Probes were inserted into the brain perpendicular to the surface and lowered to layers II/III and IV under visual guidance and based on readings from the micromanipulator (depths: between 600 and 900 μm).

Thalamic unit and LFP activities were recorded using quartz-insulated platinum/tungsten (90%/10%) microelectrodes (∼1–2 MΩ, Thomas Recording, Giessen, Germany). One to two microelectrodes were guided independently at 1 μm resolution through a five-channel concentric microdrive head (Head05-cube-305-305-b, Thomas Recording) with 305 μm inter-electrode spacing.

Raw signals were amplified (5000×) and digitized at 33,657 Hz (Neuralynx recording systems, Bozeman, MT, USA). LFPs were obtained by filtering raw signals between 0.1 and 300 Hz. For unit recordings, raw signals were filtered between 600 and 6000 Hz. Waveforms crossing set thresholds (100–120 μV) were captured via the A/D card and analysed off-line. Potential single units were first identified using automated clustering software utilizing peak and trough feature sets (KlustaKwik [Klustakwik.sourceforge.net]). These clusters were then examined manually for waveform shape (SpikeSort3D, Neuralynx). Clustering extracellular action potential waveforms from the different recording sites in a tetrode typically enabled discrimination of one to three single units. We considered as multi-unit activity (MUA) clusters that were not easily isolated.

Intracellular recordings from cortical neurons were performed with pulled glass (1.5 mm o.d.) micropipettes. Pipettes were filled with 2–3 M potassium acetate and had DC resistances of 60–80 MΩ. A high-impedance amplifier (Neurodata, Cygnus Technologies, NY, USA; low-pass filter of 10 kHz) with active bridge circuitry was used to record membrane potential fluctuations and inject current into cells.

Whisker stimulation

Before recording, whiskers were trimmed to approximately 5–7 mm. Individual whiskers were mechanically deflected using a ceramic piezo-electric bimorph stimulator (Piezo Systems, Cambridge, MA, USA) as described previously (Wilent & Contreras, 2005*a*). For each recording, a glass capillary glued to the end of the stimulator was positioned so that a single whisker rested snugly inside it. The tip of the capillary was positioned approximately 5 mm from the skin. The whisker was mechanically deflected in the rostrocaudal direction (250 μm) by applying sinusoidal waves (25–200 Hz) or band-pass filtered white noise (50–200 Hz) of 0.5 or 1 s duration to the stimulator. Stimuli were delivered at a rate of 0.2 Hz. The identity of the principal whisker was determined for each animal based on the cortical multi-unit activities. The whisker that evoked the response with the shortest onset latency and the largest number of action potentials was considered to be the principal whisker (PW). For intracellular recordings, the ability of the whisker to evoke action potentials when deflected was the primary consideration for determining the PW. Depending on the recording session, we applied 30–40 trials per stimulus condition.

Data analysis

Single units were included in the analysis if their responses were >3 Hz, sustained and had a short onset latency (10 ± 2.5 ms).

Spectral analysis was carried out using the Chronux toolbox (Bokil *et al.* 2010) under MATLAB 7.5 (MathWorks, Natick, MA, USA). Spectral powers were computed using direct multitaper estimators. For the analysis of the spike–field coherence (SFC), we binned the single trial unit spike data in 1 ms bins. We then calculated the power spectra for the binned spike and the LFP data, as well as their cross spectra, using multitaper analysis with a time–bandwidth product of TW = 3 and a width = 5 tapers. These spectra and cross-spectra were averaged over trials before calculating coherence.

To determine the degree of phase locking of sustained responses to the stimulus or gamma cycles, vector strength r was calculated according to the following formula:

$$r = \frac{L}{n} = \frac{1}{n}\sqrt{\left(\sum_{j=1}^{n}\cos\theta_j\right) + \left(\sum_{j=1}^{n}\sin\theta_j\right)^2}$$

L is the vector length, n is the total number of spikes in the phase histogram for a given stimulation frequency, θ is the phase angle at which a spike occurs: $\theta = 2\pi(t/T)$. T is the period of the stimulation frequency, and t is the time at which the spike occurs. To assess the statistical significance P of the vector strength, the Rayleigh statistic was used.

Between-conditions comparison was based on a Wilcoxon rank sum test (Mann–Whitney U test) for unpaired data or Wilcoxon signed rank test for paired data.

Results

In order to understand the encoding of high-frequency somatosensory input, we used an array of four tetrodes to record local field potentials (LFPs) and spiking activity in physiologically identified barrel cortex columns of lightly sedated adult Sprague–Dawley rats (Fig. 1*A*). Electrodes were inserted perpendicular to the cortical surface into the barrel cortex and lowered to depths between 600 and 900 μm, which correspond to layers II/III and IV (Roy *et al.* 2011).

The example in Fig. 1*B* shows a raw trace from one of the recording sites within a tetrode. We isolated LFP signals from the raw traces by low-pass filtering (0.1–300 Hz) and multi-unit spike activity (MUA) by band-pass filtering (0.6–6 kHz) and applying a threshold. Then single units were separated from the MUA using spike-sorting algorithms (Fig. 1*C*).

We deflected the principal whisker (PW) in the rostrocaudal direction with 1 s-long sinusoidal waves or white noise stimuli at frequencies ranging from 25 to 200 Hz (25 Hz increments). We used sinusoidal stimuli in similarity to Mountcastle *et al.* (1969) in order to understand frequency encoding and frequency transformations in somatosensory thalamus and cortex. We used white noise stimuli to understand whether emergent frequency transformations were also present in response to richer stimuli more similar to natural conditions. The fidelity of the stimulation device at high frequencies was measured with photodiodes. Except for a slight notch at the onset of the stimulation, we did not observe any frequency-dependent alteration in the stimulus waveform or amplitude (Fig. 1*A*; bottom traces).

The example of Fig. 1*D* shows single-trial responses from four units and the corresponding LFPs during stimulation of the PW with increasing sinusoidal frequencies. In contrast with the very few spikes generated by ramp-and-hold whisker deflections (Simons, 1978; Wilent & Contreras, 2004), single cells responded with sustained increases in spike output to the stimulation frequencies used in this study (25–200 Hz). Concomitant with the increased firing rate, the LFP recorded by the same electrode showed robust gamma (20–60 Hz) oscillations clearly visible by simple inspection of the traces (shown in the expanded traces in Fig. 1*D*, indicated by dotted lines).

Firing rate modulation and temporal patterning of cortical unit responses to high-frequency stimulation

Is the frequency of stimulation encoded by the mean firing rate of individual neurons? The peri-stimulus raster plots from four simultaneously recorded units for the entire set of stimulation frequencies are shown in Fig. 2*A*. Sensory responses were typically associated with a large increase in firing rate after stimulus onset followed by weakly adapting firing rates for the duration of the stimulus. The average mean firing rate showed a positive but very shallow slope when plotted as a function of stimulation frequency (Fig. 2*B*). However, the correlation was significant for these example units ($P < 0.03$ for the unit with the smallest R). The distribution of the correlation coefficient R for the population ($n = 104$ units from 31 animals) revealed a significant monotonic relationship between the mean firing rates and stimulation frequency for 43% of the units ($n = 45/104$; Pearson correlation coefficients >0.71; Fig. 2*C*). Therefore, in accordance with previous studies, in our recording conditions, the frequency content of whisker deflections can be encoded by the firing rate of at least a fraction of barrel cortex neurons (Arabzadeh *et al.* 2003).

Does the timing of sensory-evoked spikes contain information about the frequency of stimulation? We computed phase raster plots of the spiking activity with respect to the stimulus cycles (Fig. 2*D*). As illustrated for the example recordings, we found that the sensory-evoked spiking activity of individual neurons was often phase-locked to the sinusoidal stimuli (Fig. 2*D*).

To quantify the phase relation of spikes to the cycles of the sinusoidal stimulation, we measured the vector strength (r; see Methods) (Khatri *et al.* 2004;

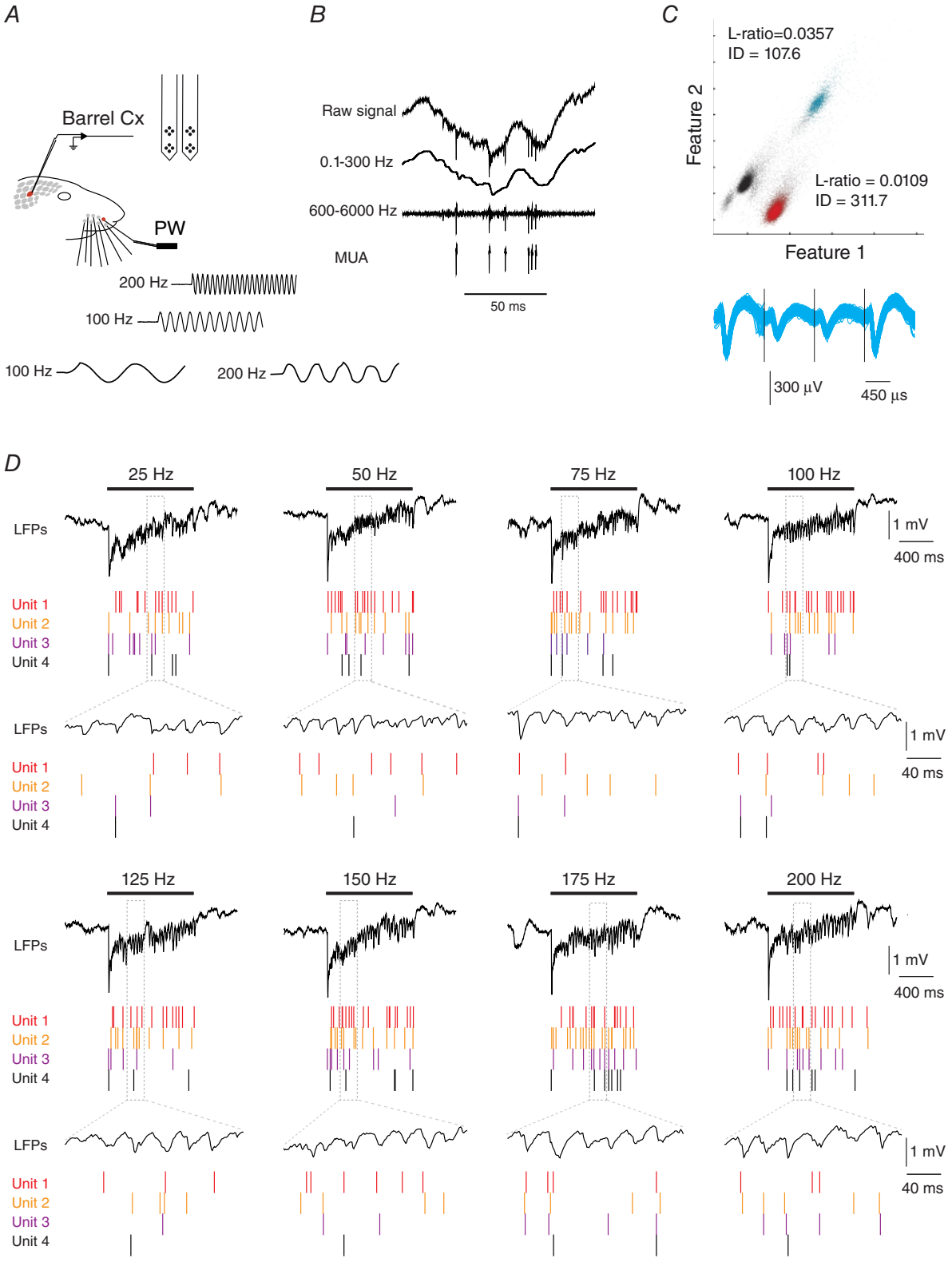

Figure 1. Simultaneous recording of sensory-evoked unit and local field potential activities in the rat barrel cortex
A, schema of the experimental protocol. Recordings were made in S1 cortex while stimulating the principal whisker (PW) using a piezo-electric device. Traces represent cutouts of the onset of some vibrotactile stimulus waveforms (100 and 200 Hz), as measured with photodiodes. *B*, filtering procedure. Upper trace corresponds to the raw signal

recorded from one of the four recording sites of a tetrode. The raw signal was low-pass filtered (0.1–300 Hz) to obtain local field potentials (LFPs, second trace), and band-pass filtered (0.6–6 kHz; third trace) to obtain the local multi-unit activity (MUA) after a thresholding procedure (bottom trace). *C*, example for the separation of MUA activity into single units. The upper graph shows spikes plotted in feature space, and colour-coded by cluster assignment. Features 1 and 2 correspond to the waveform peak values on two contacts of the tetrode. Spike cluster metrics, isolation distance, and L-ratio (Schmitzer-Torbert *et al*. 2005) are indicated for two putative single units. Non-clustered spikes are in black. Bottom, overlays of waveform values on each contact for the blue cluster. *D*, example of single-trial evoked responses for four units, recorded alongside with local field potentials during vibrotactile stimulations of the PW at different frequencies. Horizontal bars indicate stimulus presentation. Lower traces correspond to an expanded portion of the upper traces.

Ewert *et al.* 2008). A vector strength value of 1 is associated with a perfect phase locking to the stimulus cycles, whereas a vector strength value of 0 indicates a lack of a consistent phase relationship.

Although vector strength tended to decrease with increasing stimulation frequency in the example units in Fig. 2*E*, phase locking was significant for all stimulation frequencies as measured by deviation from a uniform phase–response distribution (Rayleigh test; $P < 0.05$).

At the population level ($n = 104$ units), the majority of neurons ($n = 95$, 91%) produced phase-locked responses at the lowest frequency of 25 Hz (Fig. 2*F*). The proportion of phase-locked units decreased with increasing frequency down to 42% ($n = 44$) at 200 Hz.

These results indicate that the frequency content of whisker vibrations is not encoded only by the firing rate modulation of barrel cortex neurons. Indeed, a sub-population of neurons can lock their sensory-evoked spiking activity to vibrotactile stimulation of up to 200 Hz.

Sensory-induced gamma oscillations during high-frequency somatosensory stimuli

To investigate whether vibrotactile stimulation might also elicit more complex internally generated population dynamics; we calculated the LFP power spectra using the multitaper method (Bokil *et al.* 2010).

We calculated the power spectrum of LFP signals in each trial during a 900 ms window starting 50 ms after the stimulus onset (sensory-induced power spectrum) and during a 900 ms window starting 1 s before the stimulus onset (baseline power spectrum). We then averaged the single-trial power spectra for the sensory-induced and baseline activities.

Figure 3*A* shows the LFP power spectrum as a function of the stimulation frequency for one recording site. As expected, we found that the 25 Hz stimulation evoked an increase in the LFP power spectra at the stimulus frequency (Fig. 3*A*, indicated by an asterisk) and its first harmonic (Fig. 3*A*, indicated by a star). These two spectral peaks shifted accordingly with the increasing stimulation frequency, with decreasing amplitude until becoming indistinguishable above 100 Hz (Fig. 3*A*, asterisk and star). In addition, we found that for stimulation frequencies above 25 Hz, the LFP power spectra revealed an emergent peak spanning the gamma band (20–60 Hz, indicated by arrows) when compared to the baseline LFP power spectra ($P < 0.05$; Mann–Whitney U test). As the stimulation frequency increased, the emergent peak at gamma remained constant in its frequency range.

To quantify sensory-induced gamma oscillations across animals and stimulation frequencies, we calculated the ratio between gamma power during sensory-induced and baseline activity ($n = 31$ recording sites from 31 animals; for each animal we took the recording site that exhibited the largest LFP signal). We found that 26 recording sites presented a significant sensory-induced increase in gamma power for stimulation frequencies between 75 and 200 Hz ($P < 0.05$; Mann–Whitney U test). We did not include in this analysis the results obtained with stimulation frequencies at 25 and 50 Hz because they elicited stimulus-locked LFP activity that encompass and contaminate the gamma band. For a 75 Hz stimulation frequency, there was a (2.1 ± 0.3)-fold increase in gamma power compared to baseline. This fold increase tended to become larger when increasing the frequency of the stimulation to reach a (3.8 ± 0.5)-fold increase for a 200 Hz stimulation frequency ($R = 0.92$; $P < 0.009$; Fig. 3*B*, left).

The frequency between 20 and 60 Hz that showed the maximum change in power from baseline (centre frequency) tended to decrease when increasing the stimulus frequency ($R = -0.87$; $P < 0.03$; Fig. 3*B*, centre). The gamma centre frequency was 33.6 ± 3.0 Hz for a 75 Hz stimulation frequency and 30.8 ± 3.9 Hz for a 200 Hz stimulation frequency.

Finally, we found that the amplitude of the gamma centre frequency tended to increase with the stimulation frequency ($R = 0.95$; $P < 0.003$; Fig. 3*B*, right). While it was a (3.0 ± 0.3)-fold increase for a 75 Hz stimulation frequency, it was a (6.8 ± 0.9)-fold increase for a 200 Hz stimulation frequency.

Relationship between gamma oscillations in the local field potential and the spiking activity

Is the sensory-induced gamma power in the LFP related to the spike response? To address this question, we calculated the spike–field coherence (SFC) during high-frequency tactile stimulation (Fries *et al.* 2001; Pesaran *et al.* 2002). To avoid direct spectral contamination of the LFPs by

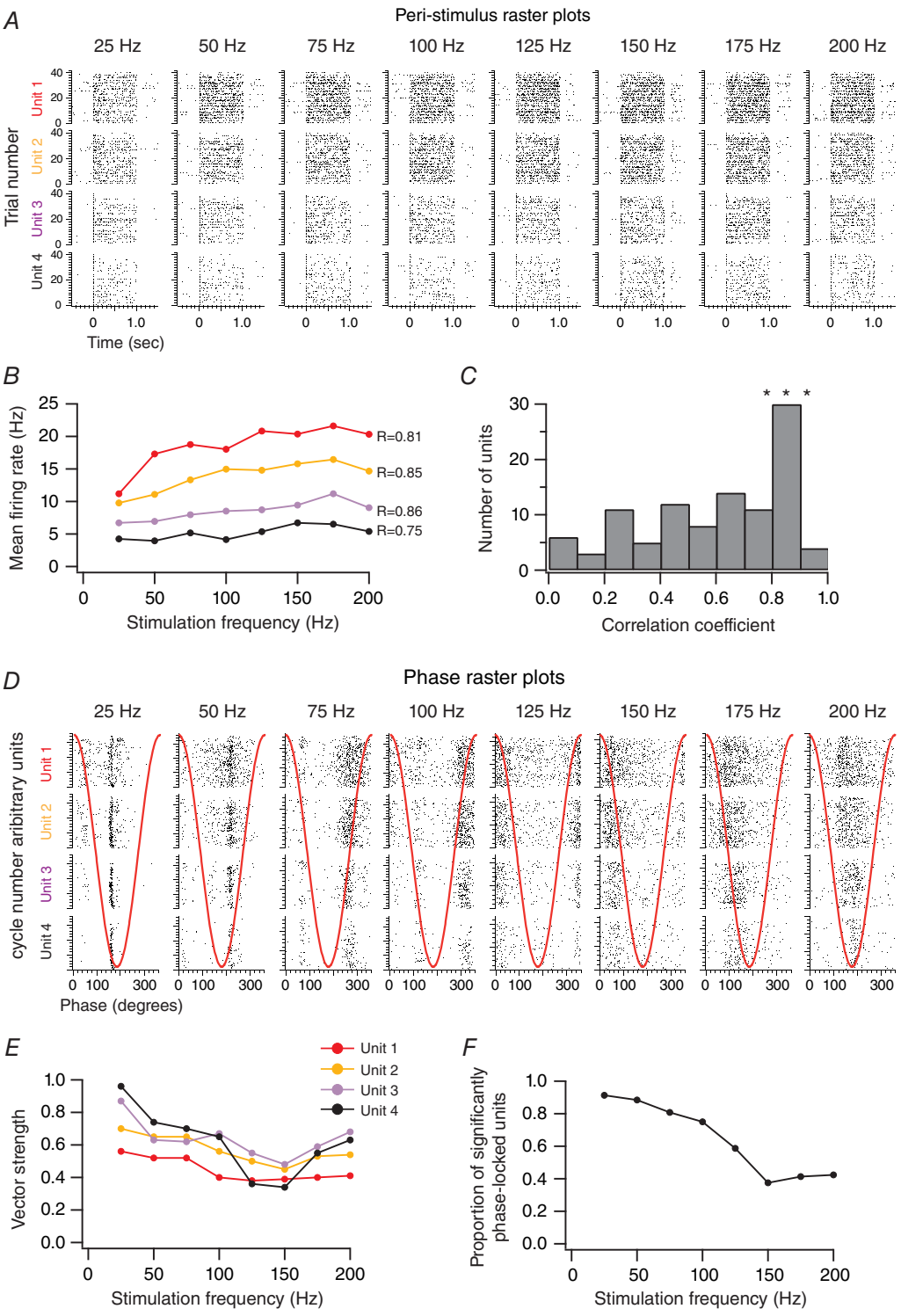

Figure 2. Responses of cortical units to high-frequency vibrotactile stimulations
A, peri-stimulus raster plots of four simultaneously recorded units to whisker stimulations of increasing frequencies. The stimulation starts at 0 s and lasts for 1 s. *B*, mean firing rate as a function of the stimulation frequency for the four simultaneously recorded units presented in *A*. *C*, distribution of the correlation coefficients between the mean firing rates and stimulation frequency for the population of recorded units (n = 104 from 31 animals). *D*, phase raster plots of the four simultaneously recorded units to whisker stimulations of increasing frequencies. Red traces illustrate one cycle of the stimulus waveform. *E*, vector strength as a function of the stimulation frequency for the four simultaneously recorded units presented in *A*. *F*, the proportion of units with a significant phase locking as a function of the stimulation frequency (n = 104 from 31 animals).

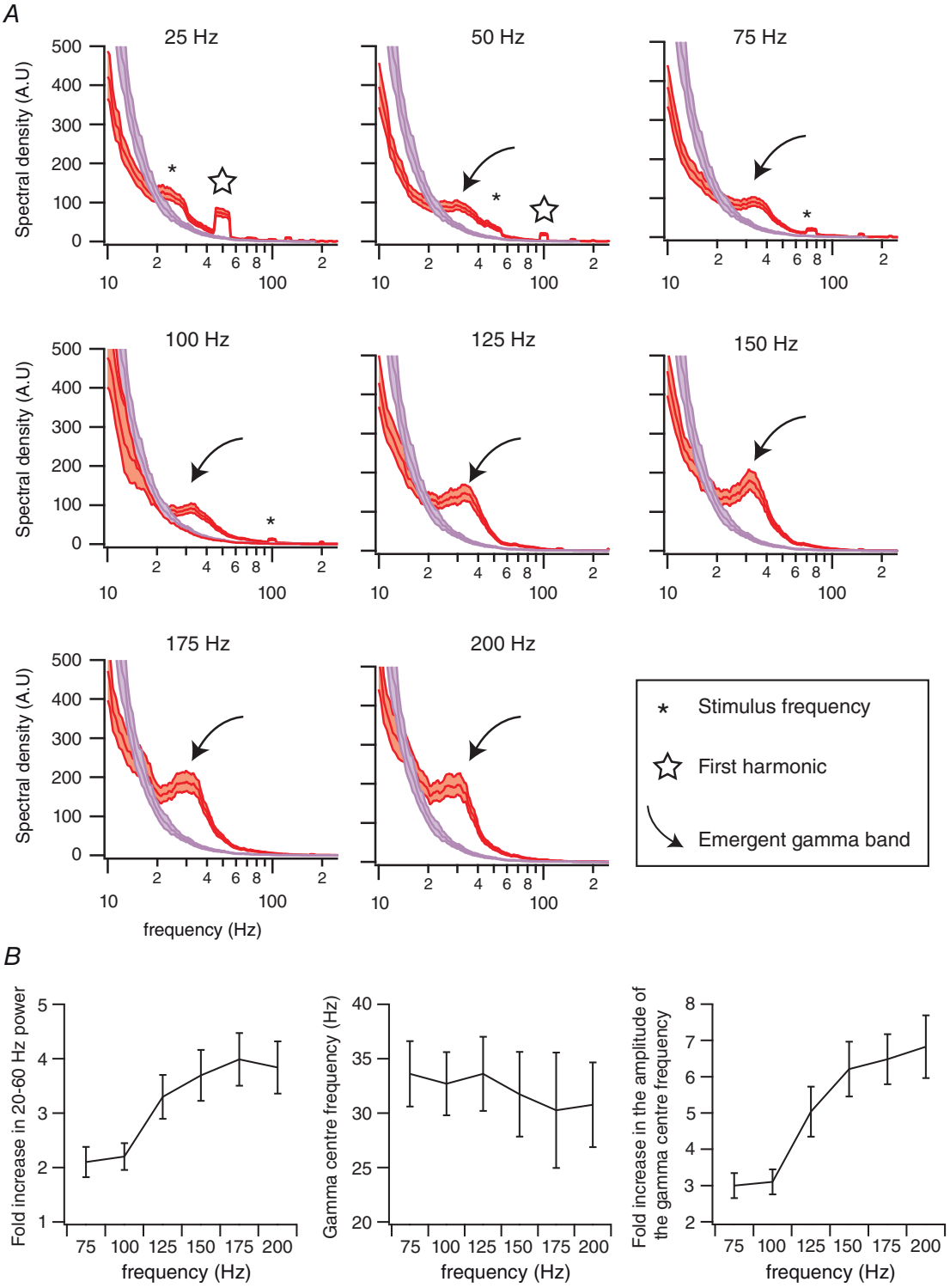

Figure 3. High-frequency vibrotactile stimuli induce gamma oscillations in the local field potentials
A, red traces correspond to the averaged power spectra for one recording site ($n = 32$ trials), computed between 50 and 950 ms after the onset of stimulus presentation. Purple traces correspond to the power spectra computed during a same duration of pre-stimulation (baseline) epochs. Shaded regions indicate the 95% error bars estimated with a jackknife across tapers and trials. *B*, left panel: fold increase in the 20–60 Hz spectral powers compared to baseline as a function of the stimulation frequency. Middle panel: gamma centre frequency as a function of the stimulation frequency. Right panel: fold increase of the gamma centre frequency as a function of the stimulation frequency. Errors bars correspond to ±1 SD. $n = 26$ recording sites from 26 animals.

spike waveforms, we used the LFPs recorded at electrodes adjacent to the one measuring spiking activity (Ray & Maunsell, 2011).

Figure 4*A* shows SFC between one unit and one recording site for baseline (Fig. 4*A*, purple) and in response to all stimulation frequencies (Fig. 4*A*, red). In close similarity to what we observed at the level of the power spectra, the 25 Hz stimulation elicited an increase in the SFC at the stimulation frequency and its first harmonic with respect to baseline. This simply reiterates the well-known fact that spike output is well time locked to the whisker stimulus. However, as stimulation frequency increased, SFC in the gamma band (20–60 Hz) first appeared in response to 50 Hz stimulation and then significantly increased compared to baseline at all stimulation frequencies (Fig. 4*A*, arrow; $P < 0.05$; Mann–Whitney *U* test).

The increase in SFC for both the stimulation and gamma band frequencies was sustained for the duration of stimuli between 75 and 200 Hz. This is clearly seen when plotting SFC as a function of both frequency and time (Fig. 4*B*). The increase in SFC appeared right after the onset of the stimulus and continued until the stimulus was turned off, independently of stimulation frequency (Fig. 4*B*, white arrow).

For each unit, we calculated the ratio of SFC at gamma band between the sensory response and baseline. We found that 61% of the units (63 of 104, 31 animals) showed a significant fold increase in sensory-induced SFC at gamma band compared to baseline for stimulation frequencies between 75 and 200 Hz ($P < 0.05$; Mann–Whitney *U* test).

For a 75 Hz stimulation frequency, the fold increase was 1.5 ± 0.2. In close similarity to LFP gamma power, this fold increase tended to become larger with increasing stimulation frequency to reach 1.75 ± 0.2 for a 200 Hz stimulation frequency ($R = 0.85$; $P < 0.04$; Fig. 4*C*, left).

Similarly to the LFP signals, the gamma centre frequency of the SFC tended to decrease when increasing the stimulus frequency ($R = -0.96$; $P < 0.003$; Fig. 4*C*, centre). The centre frequency of the SFC was 36.1 ± 7.2 Hz for a 75 Hz stimulation frequency and 30.2 ± 4.4 Hz for a 200 Hz stimulation frequency.

Finally, we found that the amplitude of the gamma centre frequency tended to increase with the stimulation frequency ($R = 0.83$; $P < 0.05$; Fig. 4*C*, right). While it was around 0.6 ± 0.05 for a 75 Hz stimulus, it increased to 0.7 ± 0.05 for a 200 Hz stimulation frequency.

The high SFC suggests a possible encoding mechanism for stimulus frequency based on the timing of spikes with respect to the gamma cycle. To test this hypothesis, we band-pass filtered the raw LFP signals (20–60 Hz) and detected the gamma cycles by applying an amplitude threshold of 2.5 SD above baseline noise (Fig. 5*A*). This procedure allowed us to measure the phase relationships between the spiking and gamma activity. The distribution of spikes evoked by vibrotactile stimuli of increasing frequencies is shown for one unit in Fig. 5*B*. We excluded the 75 Hz stimuli because of the close similarity of this frequency with the gamma band signal. For, this example unit, the mode corresponds to the bin between 60 and 120 deg for all stimulation frequencies (Fig. 5*B*, mode indicated by arrow).

The distribution of modes for all units that were associated with a significant increase in the SFC within the gamma frequency band is shown in Fig. 5*C* ($n = 63$). For most units, the preferred phases were between 60 and 180 deg, which correspond to the falling phase of the gamma cycle. Only a few units exhibited preferred phases between 180 and 240 deg, which corresponds to the trough of the gamma cycle. This distribution did not depend on the frequency of the stimulation. Therefore, sensory-induced gamma oscillations strongly modulate the spiking of cortical units; however, they do not support a stimulus-dependent spike-phase coding scheme.

Influence of gamma oscillations on the temporal precision of sensory-evoked spiking activity

Are the spikes phase-locked to gamma different from those that are phase-locked to stimulus frequency? We computed phase histograms by taking into account either all the action potentials during the response (Fig. 6*A*) or only those that concomitantly occur during a gamma cycle (Fig. 6*B*). An example of the distribution of spikes with respect to the stimulus cycles to stimuli of increasing frequencies (100–200 Hz) is illustrated in Fig. 6*A* (all spikes) and *B* (only the spikes that concomitantly occur during a gamma cycle). Even though the number of spikes is reduced, the phase locking to the stimulus is still obvious in Fig. 6*B* rasters.

We found that for a stimulation frequency of a 100 Hz, 79% of the units that presented a significant increase in the SFC at gamma frequency also have their action potentials significantly locked to the stimulus cycles (Fig. 6*C*). This proportion decreased with frequency and was 46% at 200 Hz (Fig. 6*C*). Importantly, regardless of stimulation frequency, we did not observe any difference in the proportion of units with significantly stimulus-locked responses when taking into account all their action potentials or only those occurring during a gamma cycle (Fig. 6*C*).

Similarly, the vector strength for the units that have their action potentials significantly stimulus locked at all frequencies ($n = 29$ out of 63) was not different when taking into account all their action potentials or only those occurring during a gamma cycle (Wilcoxon signed rank test; Fig. 6*D*).

This result indicates that sensory-induced gamma oscillations temporally frame the occurrence of action

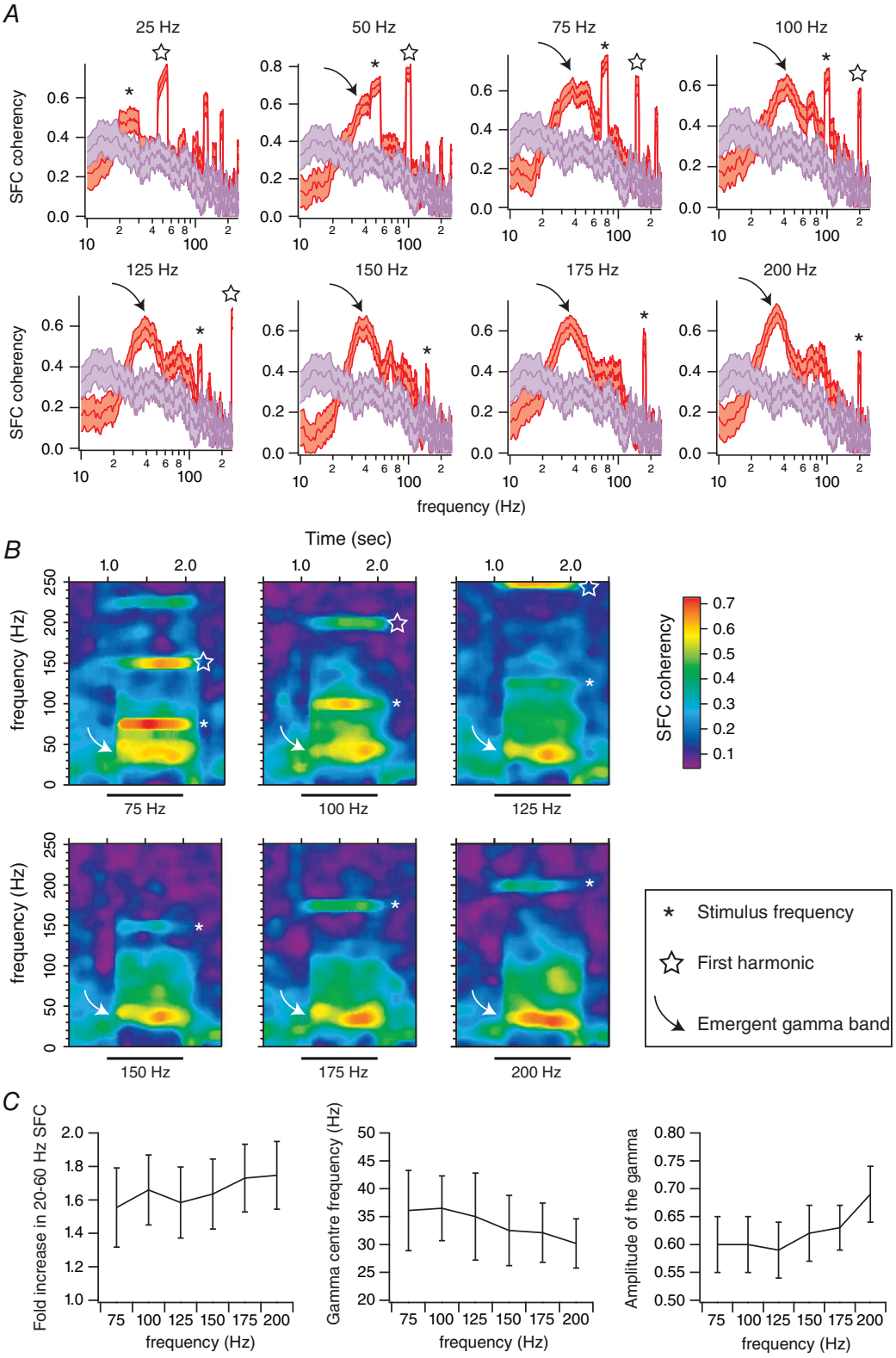

Figure 4. High-frequency vibrotactile stimuli increase the spike–field coherence in the gamma band range

A, red traces correspond to the averaged spike–field coherence (SFC) for one single unit ($n = 36$ trials), computed between 50 and 950 ms after the onset of stimulus presentation. Purple traces correspond to the spike–field coherence computed during pre-stimulation (baseline) epochs. Shaded regions indicate the 95% error bars

estimated with a jackknife across tapers and trials. *B*, average coherence between the spiking and local field potential activities across time for the unit presented in *A*. Time is on the *x*-axis; frequency is on the *y*-axis. Coherence is colour-coded on a linear scale. Horizontal bars indicate stimulus presentation. *C*, left panel: fold increase in the 20–60 Hz spike–field coherence compared to baseline as a function of the stimulation frequency. Middle panel: gamma centre frequency of the spike–field coherence as a function of the stimulation frequency. Right panel: the amplitude of the gamma centre frequency of spike–field coherence as a function of the stimulation frequency. Errors bars correspond to ±1 SD. $n = 63$ units from 26 animals.

potentials while preserving sub-millisecond phase relations with sensory inputs, and points toward the existence of coexisting temporal coding schemes that combine information across different time scales during the cortical processing of high-frequency vibrotactile stimulations.

Sub-threshold membrane potential fluctuations underlying coexisting temporal coding schemes

LFPs are mainly generated by synaptic currents, therefore the membrane potential fluctuations of layer IV barrel neurons should show the presence of synaptic potentials at both gamma and the stimulation frequency. We performed intracellular recordings from electrophysiologically identified regular spiking neurons in layer IV (Fig. 7*B*; $n = 25$). We recorded the responses to 200 Hz vibrotactile stimulation of the principal whisker at depolarized membrane potentials by slight injections of positive current (0.1–0.4 nA). Under these circumstances, stimulation of the principal whisker evoked sustained trains of action potentials not different from those recorded extracellularly (Fig. 7*C*). In 11 cells (out of 25), action potentials were precisely phase locked with stimulus cycles as assessed with a Rayleigh test (Fig. 7*F*; $P < 0.05$). In order to analyse the spectral composition of sensory-evoked membrane potential fluctuations, we used negative currents (−0.3 to −0.6 nA) to hyperpolarize these cells at membrane potentials that preclude action potential generation (Fig. 7*D*). In six cells (out of 11), power spectra revealed a sharp and significant increase both in the gamma band range (20–60 Hz) and at the frequency of the stimulation (200 Hz; Fig. 7*E*). Indeed, visual inspection of single-trial membrane potential fluctuations of those cells revealed a temporal framing of high frequency (200 Hz) stimulus-evoked excitatory postsynaptic potentials by the gamma (20–60 Hz) rhythm (Fig. 7*D*; right panel). This observation further indicates that the dual phase locking we observed in our extracellular recordings is not related to the fact that some trials are associated with precise stimulus-locked responses and others with sensory-induced gamma oscillations. Moreover, the fact that gamma band fluctuations were reliably observable at both depolarized and hyperpolarized membrane potentials (right panels of Fig. 7*C* and *D*) suggests that, in regular spiking neurons, sensory-induced gamma oscillations are in large part generated by synaptic inputs rather than intrinsic properties.

Coupling of thalamic and cortical local field potentials and spiking activity

Since intracellular recordings of cortical cells suggest that sensory-induced gamma oscillations are generated by synaptic inputs, one possibility is that thalamic inputs at gamma frequency are imposed on thalamo-recipient cortical neurons. To address this hypothesis, we performed simultaneous recordings of topographically aligned thalamic and cortical recording sites (Fig. 8*A*). We only selected experiments where cortical LFP recordings were associated with a significant increase in gamma oscillations upon a 200 Hz stimulation frequency (Fig. 8*B*; $n = 12$ out of 14 animals). As illustrated for the example dual recording in Fig. 8, the power spectrum of the LFP recorded from VPM during high-frequency whisker stimulation did not contain power in the gamma band (Fig. 8*C*, grey traces; $n = 12$ recording sites out of 12 experiments), while the cortical LFP did show a robust gamma peak (Fig. 8*C*, red traces).

Furthermore, while cortical units displayed an increase in the SFC with respect to the local LFPs in both the gamma band and the stimulus frequency (Fig. 8*D*, red traces; $n = 17$ units out of 12 animals), thalamic units displayed an increase in the SFC with respect to cortical LFPs only at the stimulus frequency (Fig. 8*D*, grey traces; $n = 17$ units out of 12 animals). As shown above, the 2-D surface plots of SFC showed a sustained increase in SFC for gamma and stimulation frequencies for the cortical recording (Fig. 8*E*, left) but only for the stimulus frequency for the thalamic recording (Fig. 8*E*, right).

These results indicate that VPM units relay precisely stimulus-locked inputs to the cortex and suggest that gamma oscillations are "de novo" generated at the level of the barrel cortex.

Sensory-evoked gamma oscillation in response to band-pass noise stimuli

Sinusoidal stimulation allowed us to conduct a parametric search of the modulation of internally generated oscillations by sensory inputs. While it has been established that rats can discriminate vibrating stimuli of different frequencies (Gerdjikov *et al.* 2010), these steady-state stimuli are rarely if ever encountered by these animals in their natural environment. Indeed, in freely behaving rats, texture exploration leads to micromotions, which contain

both resonance vibration and irregular, high-velocity motion events (Ritt *et al.* 2008).

Do irregular patterns of whisker stimulations also elicit gamma oscillations? To address this question, we investigated the cortical responses to band-pass (50–200 Hz) white noise stimuli. As illustrated for the example single-unit recording in Fig. 9*A*, repeated presentation of the same noise stimulus elicited reliable and temporally precise spiking in cortical neurons (Fig. 9*B*). Furthermore, in close similarity to what we observed with

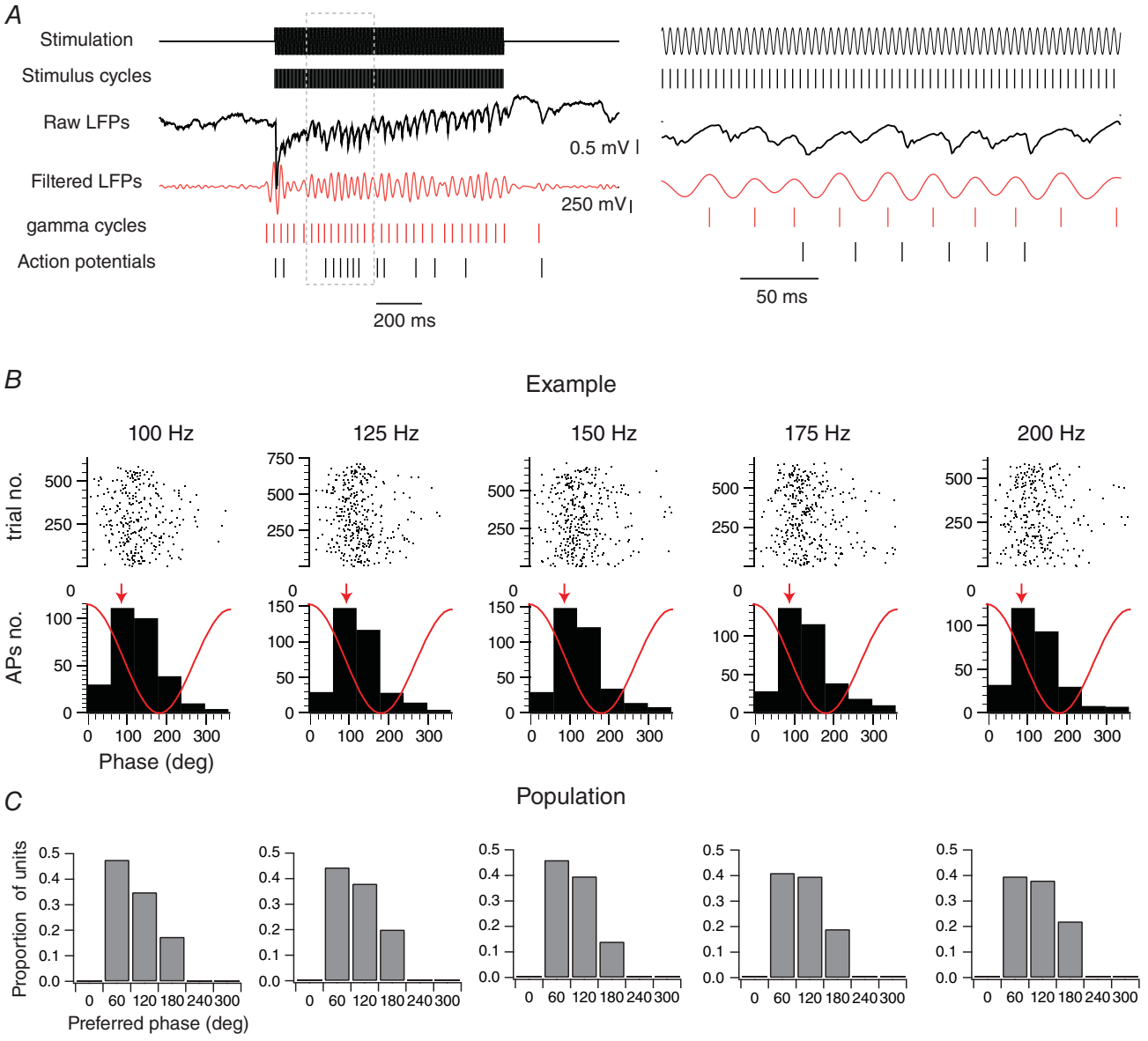

Figure 5. Gamma phase modulation of the spiking activity
A, left: an example of single-trial evoked responses of a single-unit activity recorded alongside with local field potentials during vibrotactile stimulations of the PW at 200 Hz. The upper trace corresponds to the stimulus waveform. The second line corresponds to the stimulus cycles. They were extracted by detecting the peaks of the stimulus waveforms. The third trace corresponds to the raw local field potentials. The fourth trace corresponds to the band-pass filtered (20–60 Hz) local field potentials. The gamma cycles (fifth trace) were detected by applying a threshold of 2.5 SD above the noise to the gamma peaks on the local field potentials after a band-pass filtering of 20–60 Hz. The last trace corresponds to the spiking activity of the single unit. The right panel corresponds to an expended portion of the traces on the left. *B*, raster plot and histogram representations of the spike count distribution within the gamma cycles as a function of the stimulation frequency for an example unit. Red traces illustrate the idealized waveform of the filtered local field potential. The preferred phase is indicated by a red arrow. *C*, distributions of the preferred phase within the gamma cycles of individual units as a function of the stimulation frequency ($n = 63$ from 26 animals).

sinusoidal stimuli, analysis of the spectral content of LFP fluctuations evoked by these stimuli revealed an increase in the gamma band frequency (20–60 Hz) when compared to the baseline LFP power spectra ($P < 0.05$; Mann–Whitney U test; $n = 18$ recording sites out of 18 experiments; Fig. 9*C*).

The analysis of the relationship between sensory-evoked LFPs and the spiking activity revealed that 24 out of 33 single units displayed an increase in the SFC within the gamma band frequency (Fig. 9*D*, black arrow; $P < 0.05$; Mann–Whitney U test; 18 animals), which was sustained for the duration of the stimulus (Fig. 9*E*, white arrow). Therefore, sensory-induced gamma oscillations in the barrel cortex are not specific to sinusoidal stimuli and are likely to be evoked during texture exploration.

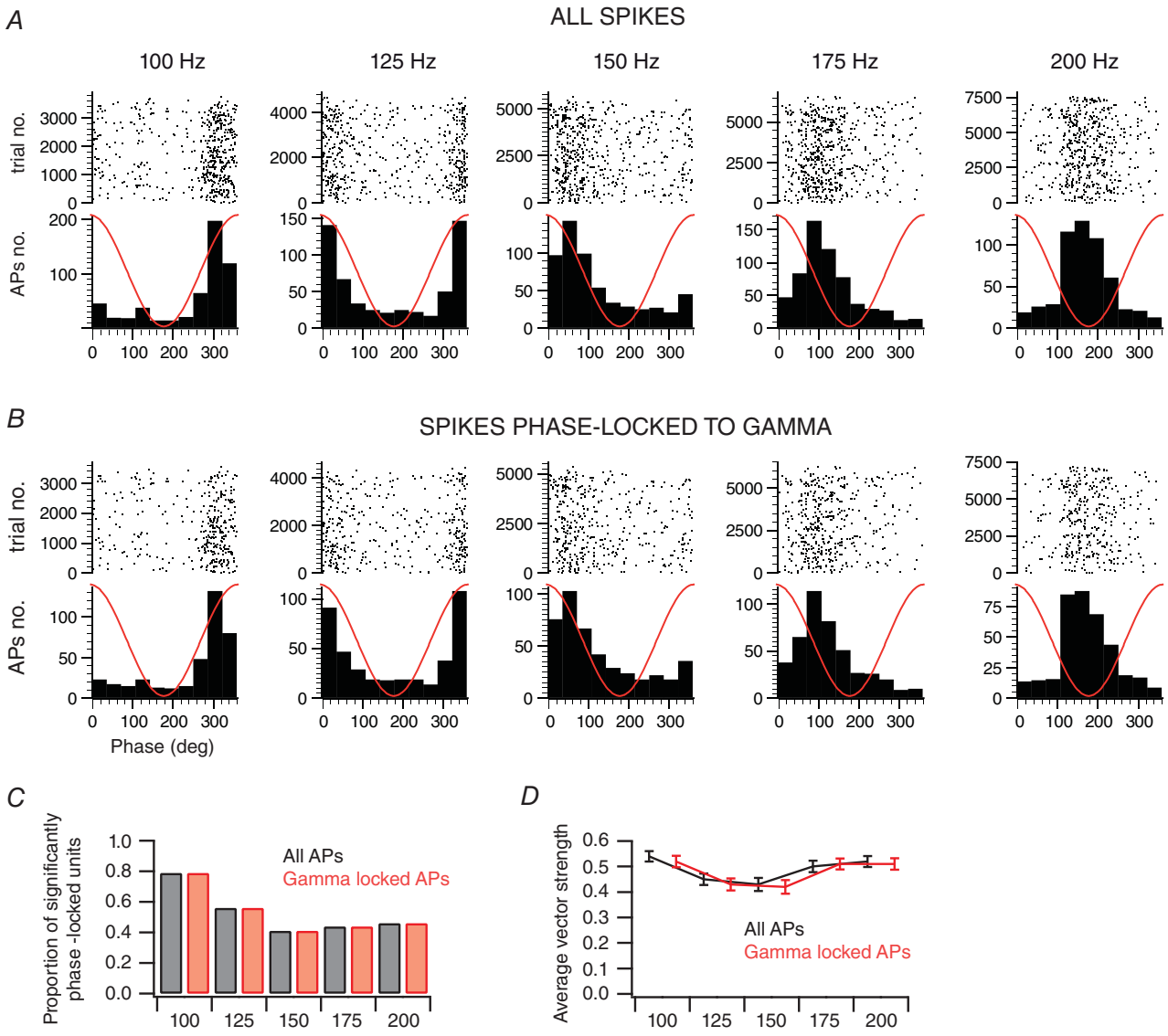

Figure 6. Sensory-induced gamma oscillations do not alter the phase relationships between the spiking activity and the stimulus cycles
A, raster plot and histogram representations of the spike count distribution within the stimulus cycles as a function of the stimulation frequency for an example unit. Red traces illustrate the stimulus waveform. *B*, for the same unit presented in *A*, raster plot and histogram representations of the spike count distribution within the stimulus cycles as a function of the frequency of the stimulation, when taking into account only the spikes that occur during gamma cycles. Red traces illustrate the stimulus waveform. *C*, the proportion of units with a significant phase locking, when considering all spikes (black) or only spikes occurring during gamma cycles (red), as a function of the stimulation frequency ($n = 63$ from 26 animals). *D*, average vector strength, when considering all spikes (black) or only spikes occurring during gamma cycles (red), as a function of the stimulation frequency. Only significantly phase-locked units for all stimulation frequencies were considered ($n = 29$ from 16 animals).

Discussion

Our goal was to identify neuronal activity in the rat barrel cortex that signals high-frequency whisker vibrations. We reasoned that behaviourally relevant high-frequency inputs must be related to specific signatures of neuronal activity in cortex. Using intra- and extracellular recordings from layer IV barrel cells in lightly sedated rats, we found a weak monotonic relationship between stimulus frequency and mean firing rate. This shallow and monotonic relation, albeit statistically significant, seems insufficient to support the fine discrimination that rats are able to achieve among textures eliciting whisker vibrations in the same frequency range. Furthermore, such coding scheme would not allow distinguishing between changes in the frequency *versus* the amplitude of the vibrations (Arabzadeh *et al.* 2003, 2004; Gerdjikov *et al.* 2010). Thus, we hypothesized that high-frequency inputs might be additionally encoded by the temporal order of the spike responses with respect to the stimulus. Indeed, we show that electrophysiologically identified regular spiking cortical neurons in layer IV of barrel cortex entrain to repetitive whisker deflections for frequencies spanning 25–200 Hz. Furthermore, we also show that high-frequency whisker stimulation triggers sustained gamma oscillations for the duration of the stimulus and more than half of layer IV barrel neurons

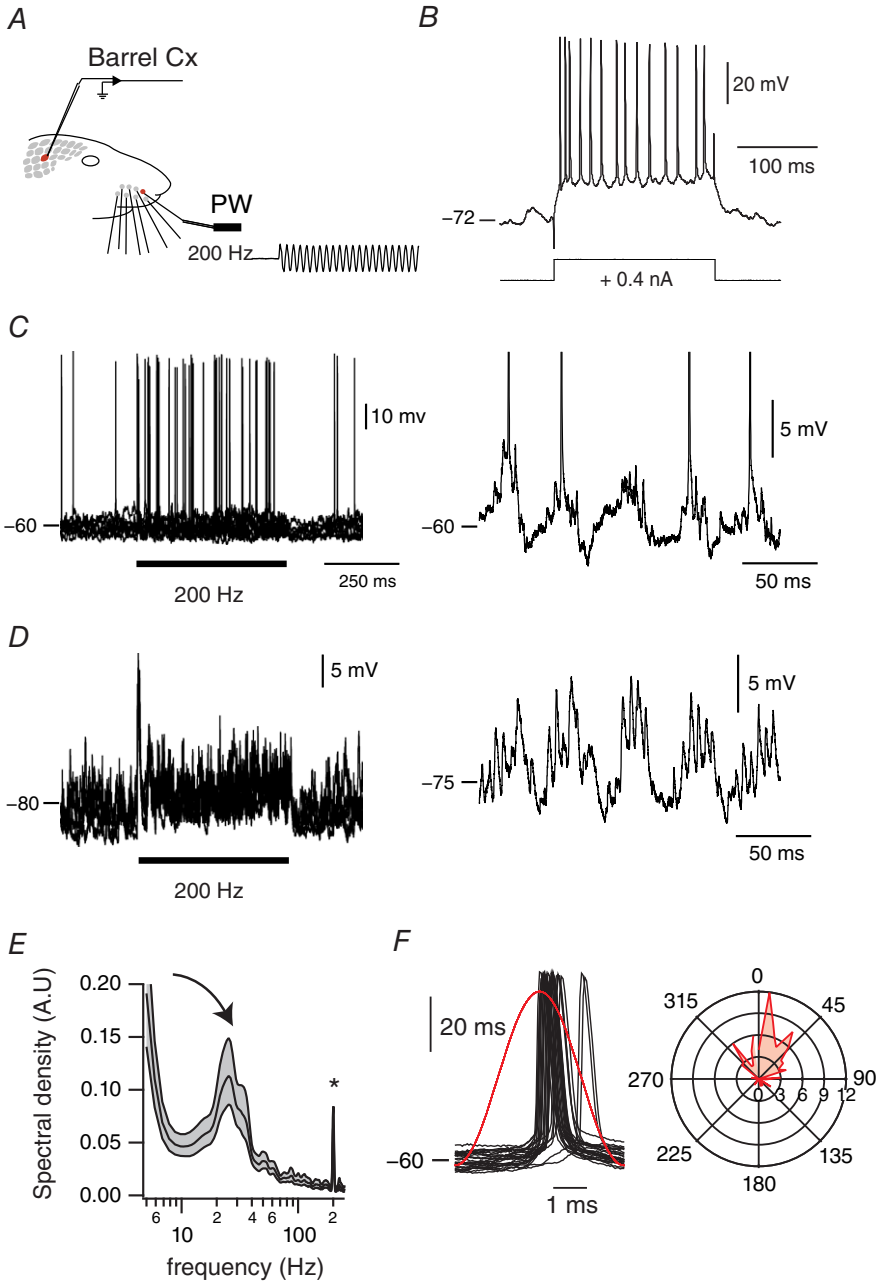

Figure 7. Sub-threshold membrane potential fluctuations underlying coexisting temporal coding schemes
A, schema of the experimental protocol. Recordings were made in S1 cortex while stimulating the PW using a piezo-electric device. The trace represents a cutout of the onset of a vibrotactile stimulus waveform at 200 Hz, as measured with photodiodes. *B*, adapting firing pattern of a regular spiking cortical cell in response to a current pulse, at rates below 100 Hz. *C*, left panel, overlay of membrane potential fluctuations in response to a 200 Hz sinusoidal whisker stimulation at depolarized membrane potentials (10 trials). Horizontal bar indicates stimulus presentation. An expanded example of the sensory-evoked activity is shown in the right panel. *D*, left panel, overlay of membrane potential fluctuations in response to a 200 Hz sinusoidal whisker stimulation when the cell was under enough hyperpolarizing current to preclude supra-threshold responses (10 trials). Horizontal bar indicates stimulus presentation. Again, an expanded example of the sensory-evoked activity is shown on the right panel. *E*, averaged power spectra of the sensory-evoked membrane potential fluctuation when the cell was held at hyperpolarized membrane potentials. The analysis was computed between 50 and 450 ms after the onset of the stimulus presentation. Shaded regions indicate the 95% error bars estimated with a jackknife across tapers and trials. Asterisk indicates the frequency of stimulation; curved arrow indicates the emergent gamma band. *F*, left panel: overlay of action potentials of the cell with respect to the stimulus cycle. Red trace illustrates the stimulus waveform. Right panel: polar plot representation of the phase relationships between all the action potentials of the cell and the stimulus cycles (50 bins). Peak location of the stimulus cycle is indicated by 0 deg.

entrain to gamma cycles. Thus, single-unit spikes entrain to both the frequency of the stimulus and the emergent gamma oscillations.

Using intracellular recordings from layer IV barrel neurons, we showed that these two frequencies coexist at the level of single cortical cells. Because our recordings show that VPM neurons fire at the frequency of the stimulus but not at gamma band frequency, we hypothesized that the EPSPs at stimulus frequency are of thalamic origin while those at gamma frequency are from neighbouring cortical cells. The lack of gamma oscillations in VPM also indicates that gamma is generated in cortex as a result of the sustained high-frequency input from thalamic cells (Barth & MacDonald, 1996).

As stimulus-locked spike patterns and spike phase with respect to gamma oscillations were highly reliable in the same epochs (Fig. 7), high-frequency (50–200 Hz) vibrotactile stimulation is encoded by two coexisting temporal coding schemes. While temporally precise spike patterns of action potentials would considerably increase

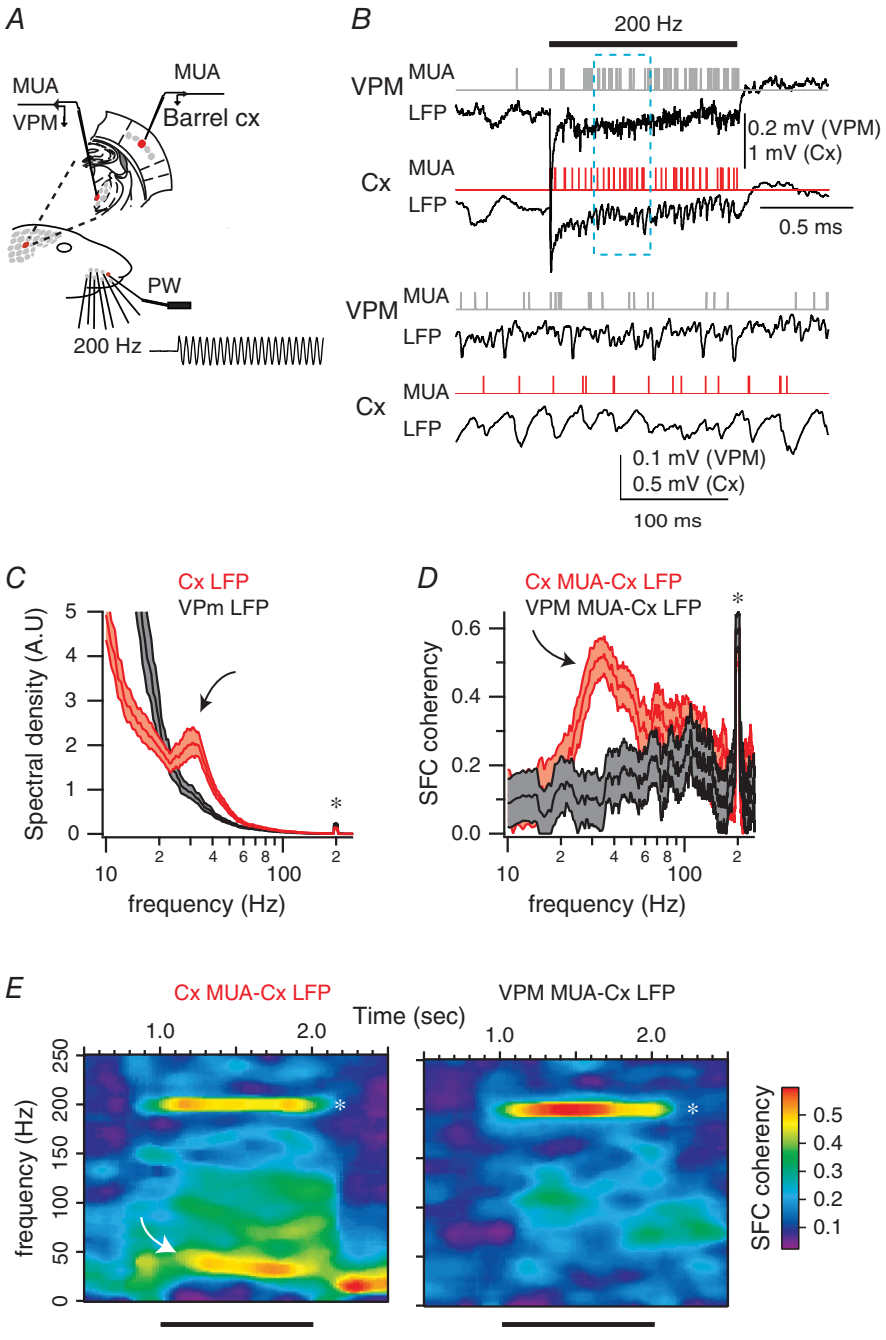

Figure 8. Lack of sensory-induced gamma oscillations in the thalamus
A, schema of the experimental protocol. Recordings were made in topographically aligned thalamic and cortical recording sites while stimulating the principal whisker using a piezo-electric device. The trace represents a cutout of the onset of a vibrotactile stimulus waveform at 200 Hz, as measured with photodiodes. *B*, example of single-trial evoked responses of topographically aligned thalamic and cortical recording sites. Horizontal bar indicates stimulus presentation. Lower traces correspond to an expended portion of the upper traces. *C*, red traces correspond to the averaged power spectra for one cortical recording site, computed between 50 and 950 ms after the onset of the stimulus presentation. Black traces correspond to the power spectra computed in a topographically aligned thalamic site recorded simultaneously with the cortical one. Shaded regions indicate the 95% error bars estimated with a jackknife across tapers and trials. Asterisk indicates stimulation frequency; curved arrow indicates emergent gamma power. *D*, red traces correspond to the averaged spike–field coherence for the cortical recording site, computed between 50 and 950 ms after the onset of stimulus presentation. Black traces correspond to the power spectra computed in a topographically aligned thalamic site recorded simultaneously with the cortical one. Shaded regions indicate the 95% error bars estimated with a jackknife across tapers and trials. Asterisk indicates stimulation frequency; curved arrow indicates emergent gamma power. *E*, average coherence of the spiking and cortical field potential activity across time for the cortical recording site (left) and the thalamic recording site (right). Time is on the *x*-axis; frequency is on the *y*-axis. Coherence is colour-coded on a linear scale. Horizontal bars indicate stimulus presentation.

the amount of information available about stimulus features when compared to the mean firing rate alone (Bialek *et al.* 1991; Reinagel & Reid, 2000; Harvey *et al.* 2013), induced gamma oscillations might support both early feature encoding and late complex cognitive functions (Varela *et al.* 2001; Wang, 2010).

Our study is similar in purpose to the pioneering study of Mountcastle's group (Hyvarinen *et al.* 1968) but results diverge in important ways. Mountcastle's group found two classes of neurons in primary somatosensory cortex of alert monkeys in response to sinusoidal stimulation of the glabrous skin of the hand. One class of cortical cell entrained its spike output, on a cycle-by-cycle basis, to low-frequency (5–50 Hz) stimulation while the other increased mean firing rate in response to high-frequency stimulation (50–400 Hz) with no temporal entrainment to the stimulus. The low-frequency cortical units, which are linked to Meissner corpuscles, increased little or not at all their mean firing rate to increasing stimulus frequency and thus Mountcastle's group concluded that these neurons could signal the sense of vibration by their ordered sequence of firing. In contrast, high-frequency responding

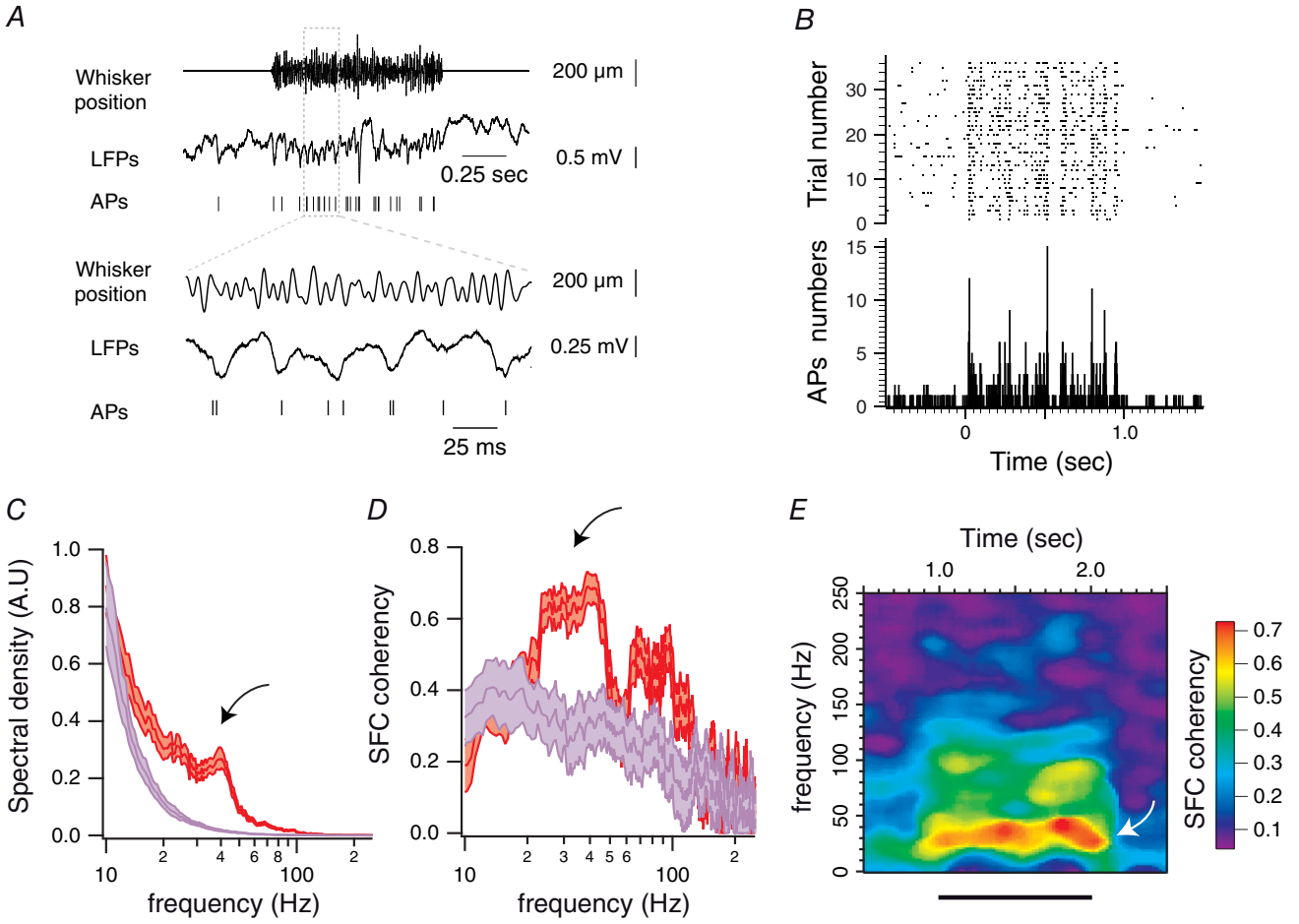

Figure 9. Sensory-induced gamma oscillations in response to band-pass noise stimuli
A, example of single-trial evoked responses for one unit, recorded alongside with local field potentials during band-pass (50–200 Hz) white noise stimulations of the PW. Lower traces correspond to an expanded portion of the upper traces. *B*, peri-stimulus raster plot and peri-stimulus time histogram of one recorded unit in response to band-pass (50–200 Hz) white noise stimulation of the PW. The stimulation starts at 0 s and lasts for 1 s. *C*, red traces correspond to the averaged power spectra for one recording site ($n = 32$ trials), computed between 50 and 950 ms after the onset of stimulus presentation. Purple traces correspond to the power spectra computed during a same duration of pre-stimulation (baseline) epochs. Shaded regions indicate the 95% error bars estimated with a jackknife across tapers and trials. Curved arrow indicates gamma band. *D*, red traces correspond to the averaged spike–field coherence for one single unit ($n = 36$ trials), computed between 50 and 950 ms after the onset of the stimulus presentation. Purple traces correspond to the spike–field coherence computed during pre-stimulation (baseline) epochs. Shaded regions indicate the 95% error bars estimated with a jackknife across tapers and trials. Curved arrow as in *C*. *E*, average coherence between the spiking and local field potential activities across time for the unit presented in *A*. Time is on the *x*-axis; frequency is on the *y*-axis. Coherence is colour coded on a linear scale. Horizontal bars indicate stimulus presentation. Curved arrow as in *C*.

units, which are linked to Pacinian corpuscles, could signal vibration frequency by increasing firing rate, working as a labelled line. In contrast, in our study, we found 43% of units that entrained to high frequencies and may thus represent a different functional class. Furthermore, almost all neurons entrained to the lower frequency of 25 Hz and thus, the high-frequency entraining units seem to indeed represent a unique class of neurons with a surprisingly broad band of frequency entrainment. We conclude that, in the barrel cortex, the frequency of whisker vibration is represented by at least two types of neurons: broadband units, which entrain to low- and high-frequency stimulation (43%), and low-frequency units, which do not entrain to high-frequency stimulation. How these functional responses emerge from a single type of rapidly adapting peripheral fibre (Jones *et al.* 2004; Sakurai *et al.* 2013) is the subject of future experiments.

Functional significance of sensory-induced gamma oscillation

In the visual system, oscillations in the gamma frequency band (Eckhorn *et al.* 1988; Gray & Singer, 1989) have been proposed as a mechanism by which activity patterns in spatially separate regions of the brain are temporally coordinated (Gray *et al.* 1989). Temporal coordination appears as synchronous firing among cell assemblies that are formed dynamically in response to specific characteristics of the sensory stimulus.

While the hypothesis of "binding by synchrony" is quite controversial (Shadlen & Newsome, 1998; Ray & Maunsell, 2010), a recent study indicates that synchronous firing at gamma frequency generates stronger signals in subsequent processing stages, thus transferring specific patterns of network activation (Jia *et al.* 2013). At the cellular level, presynaptic synchrony might enhance information transfer by reducing spike threshold and increasing the probability of spike generation (Azouz & Gray, 2003; Wilent & Contreras, 2005*b*). At the network level, synchronized gamma frequency input can also act to suppress responses in downstream elements to competing inputs that are less synchronized or out phase (Börgers & Kopell, 2008; Cardin *et al.* 2009; Akam & Kullmann, 2010). At the behavioural level, enhanced synchronization at gamma frequencies in primate visual cortex is correlated with faster task reaction times (Womelsdorf *et al.* 2005; Ni *et al.* 2016). In addition, optogenetically induced gamma oscillations in the somatosensory cortex can enhance the detection of tactile stimuli (Siegle *et al.* 2014). It is noteworthy that the interaction between gamma oscillations and spiking activity seems to play a central role in attentional modulation of sensory inputs (Fries *et al.* 2001; Chalk *et al.* 2010).

Potential mechanisms underlying sensory-induced gamma oscillations

Despite their hypothesized importance, the cellular mechanisms underlying the phenomena of sensory-induced gamma oscillation remain poorly understood. As in the studies on stimulus-induced gamma oscillations in the visual system (Gray & Singer, 1989; Castelo-Branco *et al.* 1998; Bastos *et al.* 2014), our results emphasize the purely intracortical synchronization of these oscillations and their absence in the corresponding thalamic relay.

The fact that in our recordings the spiking of cortical neurons is precisely phase locked to both the stimulus and the cortically generated gamma oscillations raises the question of the mechanisms underlying the coexistence of these two coding schemes. One possibility is that stimulus-locked and cortically generated inputs arrive at different cellular compartments. Indeed, modelling studies showed that if both stimulus-locked and internally generated inputs arrive at the same compartment, stimulus locking would be disrupted (Thomas *et al.* 2003). However, if the two inputs are spatially segregated, interactions might be weaker and stimulus-locked patterns would be maintained (Tiesinga *et al.* 2008). Alternatively, gamma oscillations themselves might be reliably modulated by the stimulus-locked thalamic inputs (Kayser *et al.* 2009; Alenda *et al.* 2010).

It is likely that multiple mechanisms might have some contribution to the generation of sensory-induced gamma oscillation and that their relative importance will vary dynamically and spatially (Welle & Contreras, 2016). Our experiments were not designed to specifically discriminate between mechanisms but rather to characterize the cellular and network activity underlying sensory-induced gamma oscillations in the somatosensory cortex. In this way, our results are not contingent upon specific mechanisms and may be reinterpreted as necessary in the light of new hypotheses.

Relevance to schizophrenia

Several studies suggest that disruption in sensory-induced gamma oscillations are directly implicated in the cognitive abnormalities of schizophrenia (Uhlhaas & Singer, 2010). For example, the perception of illusory figures or the detection of images that requires the grouping of stimulus elements into coherent object representations, which are normally associated with synchronized gamma band oscillations recorded from occipital scalp electrodes, is disrupted in schizophrenia (Spencer *et al.* 2004; Uhlhaas *et al.* 2006).

Most studies of gamma oscillations utilize visual stimuli. However, these and other results indicate that gamma rhythm generation in the visual cortex represents a general principle of sensory encoding, which may also be

studied in primary somatosensory cortex. This is of great relevance because most genetic models of endophenotypes of schizophrenia are rodent models (Ross *et al.* 2006; Rosen *et al.* 2015) in which the most prominent sensory area is the portion of the somatosensory cortex that represents information related to the activity of the whiskers, i.e. the barrel cortex (Feldmeyer *et al.* 2013).

References

Akam T & Kullmann DM (2010). Oscillations and filtering networks support flexible routing of information. *Neuron* **67**, 308–320.

Alenda A, Molano-Mazón M, Panzeri S & Maravall M (2010). Sensory input drives multiple intracellular information streams in somatosensory cortex. *J Neurosci* **30**, 10872–10884.

Arabzadeh E, Panzeri S & Diamond ME (2004). Whisker vibration information carried by rat barrel cortex neurons. *J Neurosci* **24**, 6011–6020.

Arabzadeh E, Petersen RS & Diamond ME (2003). Encoding of whisker vibration by rat barrel cortex neurons: implications for texture discrimination. *J Neurosci* **23**, 9146–9154.

Azouz R & Gray CM (2003). Adaptive coincidence detection and dynamic gain control in visual cortical neurons in vivo. *Neuron* **37**, 513–523.

Barth DS & MacDonald KD (1996). Thalamic modulation of high-frequency oscillating potentials in auditory cortex. *Nature* **383**, 78–81.

Bastos AM, Briggs F, Alitto HJ, Mangun GR & Usrey WM (2014). Simultaneous recordings from the primary visual cortex and lateral geniculate nucleus reveal rhythmic interactions and a cortical source for γ-band oscillations. *J Neurosci* **34**, 7639–7644.

Bialek W, Rieke F, de Ruyter van Steveninck RR & Warland D (1991). Reading a neural code. *Science* **252**, 1854–1857.

Bokil H, Andrews P, Kulkarni JE, Mehta S & Mitra PP (2010). Chronux: a platform for analyzing neural signals. *J Neurosci Methods* **192**, 146–151.

Börgers C & Kopell NJ (2008). Gamma oscillations and stimulus selection. *Neural Comput* **20**, 383–414.

Buonomano DV & Maass W (2009). State-dependent computations: spatiotemporal processing in cortical networks. *Nat Rev Neurosci* **10**, 113–125.

Cardin JA, Carlén M, Meletis K, Knoblich U, Zhang F, Deisseroth K, Tsai L-H & Moore CI (2009). Driving fast-spiking cells induces gamma rhythm and controls sensory responses. *Nature* **459**, 663–667.

Castelo-Branco M, Neuenschwander S & Singer W (1998). Synchronization of visual responses between the cortex, lateral geniculate nucleus, and retina in the anesthetized cat. *J Neurosci* **18**, 6395–6410.

Chalk M, Herrero JL, Gieselmann MA, Delicato LS, Gotthardt S & Thiele A (2010). Attention reduces stimulus-driven gamma frequency oscillations and spike field coherence in V1. *Neuron* **66**, 114–125.

Deschênes M, Timofeeva E & Lavallée P (2003). The relay of high-frequency sensory signals in the whisker-to-barreloid pathway. *J Neurosci* **23**, 6778–6787.

Destexhe A & Contreras D (2006). Neuronal computations with stochastic network states. *Science* **314**, 85–90.

Diamond ME, von Heimendahl M, Knutsen PM, Kleinfeld D & Ahissar E (2008). 'Where' and 'what' in the whisker sensorimotor system. *Nat Rev Neurosci* **9**, 601–612.

Eckhorn R, Bauer R, Jordan W, Brosch M, Kruse W, Munk M & Reitboeck HJ (1988). Coherent oscillations: a mechanism of feature linking in the visual cortex? *Biol Cybern* **60**, 121–130.

Ewert TAS, Möller J, Engel AK & Vahle-Hinz C (2015). Wideband phase locking to modulated whisker vibration point to a temporal code for texture in the rat's barrel cortex. *Exp Brain Res* **233**, 2869–2882.

Ewert TAS, Vahle-Hinz C & Engel AK (2008). High-frequency whisker vibration is encoded by phase-locked responses of neurons in the rat's barrel cortex. *J Neurosci* **28**, 5359–5368.

Feldmeyer D, Brecht M, Helmchen F, Petersen CCCH, Poulet JFA, Staiger JF, Luhmann HJ & Schwarz C (2013). Barrel cortex function. *Prog Neurobiol* **103**, 3–27.

Freeman AW & Johnson KO (1982). Cutaneous mechanoreceptors in macaque monkey: temporal discharge patterns evoked by vibration, and a receptor model. *J Physiol* **323**, 21–41.

Fries P, Reynolds JH, Rorie AE & Desimone R (2001). Modulation of oscillatory neuronal synchronization by selective visual attention. *Science* **291**, 1560–1563.

Gerdjikov TV, Bergner CG, Stüttgen MC, Waiblinger C & Schwarz C (2010). Discrimination of vibrotactile stimuli in the rat whisker system: behavior and neurometrics. *Neuron* **65**, 530–540.

Gray CM & Singer W (1989). Stimulus-specific neuronal oscillations in orientation columns of cat visual cortex. *Proc Natl Acad Sci USA* **86**, 1698–1702.

Gray CM, König P, Engel AK & Singer W (1989). Oscillatory responses in cat visual cortex exhibit inter-columnar synchronization which reflects global stimulus properties. *Nature* **338**, 334–337.

Harvey MA, Saal HP, Dammann JF III & Bensmaia SJ (2013). Multiplexing stimulus information through rate and temporal codes in primate somatosensory cortex. *PLoS Biol* **11**, e1001558.

Hasenstaub A, Sachdev RNS & McCormick DA (2007). State changes rapidly modulate cortical neuronal responsiveness. *J Neurosci* **27**, 9607–9622.

Hyvarinen J, Sakata H, Talbot WH & Mountcastle VB (1968). Neuronal coding by cortical cells of the frequency of oscillating peripheral stimuli. *Science* **162**, 1130–1132.

Jia X, Tanabe S & Kohn A (2013). γ and the coordination of spiking activity in early visual cortex. *Neuron* **77**, 762–774.

Jones LM, Depireux DA, Simons DJ & Keller A (2004). Robust temporal coding in the trigeminal system. *Science* **304**, 1986–1989.

Kayser C, Montemurro MA, Logothetis NK & Panzeri S (2009). Spike-phase coding boosts and stabilizes information carried by spatial and temporal spike patterns. *Neuron* **61**, 597–608.

Khatri V, Hartings JA & Simons DJ (2004). Adaptation in thalamic barreloid and cortical barrel neurons to periodic whisker deflections varying in frequency and velocity. *J Neurophysiol* **92**, 3244–3254.

Lottem E & Azouz R (2009). Mechanisms of tactile information transmission through whisker vibrations. *J Neurosci* **29**, 11686–11697.

Manfredi LR, Saal HP, Brown KJ, Zielinski MC, Dammann JF 3rd, Polashock VS & Bensmaia SJ (2014). Natural scenes in tactile texture. *J Neurophysiol* **111**, 1792–1802.

Mountcastle VB, Talbot WH, Darian-Smith I & Kornhuber HH (1967). Neural basis of the sense of flutter-vibration. *Science* **155**, 597–600.

Mountcastle VB, Talbot WH, Sakata H & Hyvarinen J (1969). Cortical neuronal mechanisms in flutter-vibration studied in unanesthetized monkeys. Neuronal periodicity and frequency discrimination. *J Neurophysiol* **32**, 452–484.

Ni J, Wunderle T, Lewis CM, Desimone R, Diester I & Fries P (2016). Gamma-rhythmic gain modulation. *Neuron* **92**, 240–251.

Pesaran B, Pezaris JS, Sahani M, Mitra PP & Andersen RA (2002). Temporal structure in neuronal activity during working memory in macaque parietal cortex. *Nat Neurosci* **5**, 805–811.

Ray S & Maunsell JHR (2010). Differences in gamma frequencies across visual cortex restrict their possible use in computation. *Neuron* **67**, 885–896.

Ray S & Maunsell JHR (2011). Different origins of gamma rhythm and high-gamma activity in macaque visual cortex. *PLoS Biol* **9**, e1000610.

Reinagel P & Reid RC (2000). Temporal coding of visual information in the thalamus. *J Neurosci* **20**, 5392–5400.

Ritt JT, Andermann ML & Moore CI (2008). Embodied information processing: vibrissa mechanics and texture features shape micromotions in actively sensing rats. *Neuron* **57**, 599–613.

Rosen AM, Spellman T & Gordon JA (2015). Electrophysiological endophenotypes in rodent models of schizophrenia and psychosis. *Biol Psychiatry* **77**, 1041–1049.

Ross CA, Margolis RL, Reading SAJ, Pletnikov M & Coyle JT (2006). Neurobiology of schizophrenia. *Neuron* **52**, 139–153.

Roy NC, Bessaïh T & Contreras D (2011). Comprehensive mapping of whisker-evoked responses reveals broad, sharply tuned thalamocortical input to layer 4 of barrel cortex. *J Neurophysiol* **105**, 2421–2437.

Sakurai K, Akiyama M, Cai B, Scott A, Han B-X, Takatoh J, Sigrist M, Arber S & Wang F (2013). The organization of submodality-specific touch afferent inputs in the vibrissa column. *Cell Rep* **5**, 87–98.

Shadlen MN & Newsome WT (1998). The variable discharge of cortical neurons: implications for connectivity, computation, and information coding. *J Neurosci* **18**, 3870–3896.

Siegle JH, Pritchett DL & Moore CI (2014). Gamma-range synchronization of fast-spiking interneurons can enhance detection of tactile stimuli. *Nat Neurosci* **17**, 1371–1379.

Simons DJ (1978). Response properties of vibrissa units in rat SI somatosensory neocortex. *J Neurophysiol* **41**, 798–820.

Schmitzer-Torbert N, Jackson J, Henze D, Harris K & Redish AD (2005). Quantitative measures of cluster quality for use in extracellular recordings. *Neuroscience* **131**, 1–11.

Spencer KM, Nestor PG, Perlmutter R, Niznikiewicz MA, Klump MC, Frumin M, Shenton ME & McCarley RW (2004). Neural synchrony indexes disordered perception and cognition in schizophrenia. *Proc Natl Acad Sci USA* **101**, 17288–17293.

Talbot WH, Darian-Smith I, Kornhuber HH & Mountcastle VB (1968). The sense of flutter-vibration: comparison of the human capacity with response patterns of mechanoreceptive afferents from the monkey hand. *J Neurophysiol* **31**, 301–334.

Thomas PJ, Tiesinga PHE, Fellous J-M & Sejnowski TJ (2003). Reliability and bifurcation in neurons driven by multiple sinusoids. *Neurocomputing* **52–54**, 955–961.

Tiesinga P, Fellous J-M & Sejnowski TJ (2008). Regulation of spike timing in visual cortical circuits. *Nat Rev Neurosci* **9**, 97–107.

Uhlhaas PJ, Linden DEJ, Singer W, Haenschel C, Lindner M, Maurer K & Rodriguez E (2006). Dysfunctional long-range coordination of neural activity during Gestalt perception in schizophrenia. *J Neurosci* **26**, 8168–8175.

Uhlhaas PJ & Singer W (2010). Abnormal neural oscillations and synchrony in schizophrenia. *Nat Rev Neurosci* **11**, 100–113.

Varela F, Lachaux JP, Rodriguez E & Martinerie J (2001). The brainweb: phase synchronization and large-scale integration. *Nat Rev Neurosci* **2**, 229–239.

Vinck M, Bos JJ, Van Mourik-Donga LA, Oplaat KT, Klein GA, Jackson JC, Gentet LJ & Pennartz CMA (2015). Cell-type and state-dependent synchronization among rodent somatosensory, visual, perirhinal cortex, and hippocampus CA1. *Front Syst Neurosci* **9**, 187.

Wang X-J (2010). Neurophysiological and computational principles of cortical rhythms in cognition. *Physiol Rev* **90**, 1195–1268.

Weber AI, Saal HP, Lieber JD, Cheng J-W, Manfredi LR, Dammann JF & Bensmaia SJ (2013). Spatial and temporal codes mediate the tactile perception of natural textures. *Proc Natl Acad Sci USA* **110**, 17107–17112.

Welle CG & Contreras D (2016). Sensory-driven and spontaneous gamma oscillations engage distinct cortical circuitry. *J Neurophysiol* **115**, 1821–1835.

Wilent WB & Contreras D (2004). Synaptic responses to whisker deflections in rat barrel cortex as a function of cortical layer and stimulus intensity. *J Neurosci* **24**, 3985–3998.

Wilent WB & Contreras D (2005*a*). Dynamics of excitation and inhibition underlying stimulus selectivity in rat somatosensory cortex. *Nat Neurosci* **8**, 1364–1370.

Wilent WB & Contreras D (2005*b*). Stimulus-dependent changes in spike threshold enhance feature selectivity in rat barrel cortex neurons. *J Neurosci* **25**, 2983–2991.

Wolfe J, Hill DN, Pahlavan S, Drew PJ, Kleinfeld D & Feldman DE (2008). Texture coding in the rat whisker system: slip-stick versus differential resonance. *PLoS Biol* **6**, e215.

Womelsdorf T, Fries P, Mitra PP & Desimone R (2005). Gamma-band synchronization in visual cortex predicts speed of change detection. *Nature* **439**, 733–736.

Additional information

Competing interests

None declared.

Author contributions

T.B., M.J.H. and D.C. designed the study. T.B. and M.J.H. performed the experiments. T.B. analysed all the data. T.B. and D.C. wrote the paper. All authors have approved the final version of the manuscript and agree to be accountable for all aspects of the work. All persons designated as authors qualify for authorship, and all those who qualify for authorship are listed. The experiments were carried out in Diego Contreras' lab at the University of Pennsylvania.

Funding

This work was supported by P50-MH-064045 (D.C.). T.B. was supported by the Fondation pour la Recherche Médicale (SPE20070709864).

Acknowledgements

We thank Pierre-Olivier Polack and Larry Palmer for thoughtful discussions.